

Power and limitations of single-qubit native quantum neural networks

Zhan Yu,¹ Hongshun Yao,¹ Mujin Li,¹ and Xin Wang^{1,*}

¹*Institute for Quantum Computing, Baidu Research, Beijing 100193, China[†]*

Quantum neural networks (QNNs) have emerged as a leading strategy to establish applications in machine learning, chemistry, and optimization. While the applications of QNN have been widely investigated, its theoretical foundation remains less understood. In this paper, we formulate a theoretical framework for the expressive ability of data re-uploading quantum neural networks that consist of interleaved encoding circuit blocks and trainable circuit blocks. First, we prove that single-qubit quantum neural networks can approximate any univariate function by mapping the model to a partial Fourier series. Beyond previous works' understanding of existence, we in particular establish the exact correlations between the parameters of the trainable gates and the working Fourier coefficients, by exploring connections to quantum signal processing. Second, we discuss the limitations of single-qubit native QNNs on approximating multivariate functions by analyzing the frequency spectrum and the flexibility of Fourier coefficients. We further demonstrate the expressivity and limitations of single-qubit native QNNs via numerical experiments. As applications, we introduce natural extensions to multi-qubit quantum neural networks, which exhibit the capability of classifying real-world multi-dimensional data. We believe these results would improve our understanding of QNNs and provide a helpful guideline for designing powerful QNNs for machine learning tasks.

I. INTRODUCTION

Quantum computing is a technology that exploits the laws of quantum mechanics to solve complicated problems much faster than classical computers. It has been applied in areas such as breaking cryptographic systems [1], searching databases [2], and quantum simulation [3, 4], in which it gives a quantum speedup over the best known classical algorithms. With the fast development of quantum hardware, recent results [5–7] have shown quantum advantages in specific tasks. An emerging direction is to investigate if quantum computing can offer quantum advantages in artificial intelligence, giving rise to an interdisciplinary area called *quantum machine learning* [8].

A leading strategy to quantum machine learning uses *quantum neural networks* (QNNs), which are quantum analogs of artificial neural networks (NNs). Much progress has been made in applications of QNN in various topics [9–11], including quantum autoencoder [12, 13], supervised learning [14–17], dynamic learning [18–20], quantum chemistry [21], and quantum metrology [22–24]. Similar to the field of machine learning, a crucial challenge of quantum machine learning is to design powerful and efficient QNN models for quantum learning tasks, which requires a theoretical understanding of how structural properties of QNN may affect its expressive power.

The expressive power of a QNN model can be characterized by the function classes that it can approximate. In recent times, the universal approximation property (UAP) of QNN models has been investigated, which is similar to the universal approximation theorem [25, 26] in machine learning theory. The authors of [27] suggested that a QNN model can be written as a partial Fourier series in the data and proved the existence of a multi-qubit QNN model that can realize a universal function approximator. Another work [28] considered multi-qubit QNN models as polynomials and obtained the UAP by using the Stone-Weierstrass theorem. The authors also proved UAP for single-qubit QNNs, while the input data is restricted to a finite set. Ref. [29] proved that even a single-qubit QNN can approximate any bounded function.

The above results of UAP show that the expressivity of QNNs is strong, but it does not reveal the relationship between the structural properties of a QNN and its expressive ability. Therefore the UAP may not be a

* wangxin73@baidu.com

[†] Z. Y., H. Y., M. L. contributed equally to this work.

good guide for constructing QNN models with practical interests. In particular, it is worth noting that the existence proof in Ref. [27] is under the assumption of exponential circuit depth and arbitrary observables, which does not explicitly give the structure of QNNs. Meanwhile, Refs. [28, 29] demonstrated the construction of QNNs in detail, but trainable weights are introduced in the data pre-processing or post-processing, making the models hybrid classical-quantum neural networks (hybrid QNNs) rather than native QNN models. It is unclear whether the powerful expressivity comes from the classical part or the quantum part of hybrid models. On the other hand, a systematic analysis of how parameters in the QNN affect the classes of functions that it can approximate is missing. The absence of these theoretical foundations hinders the understanding on the expressive power and limitation of QNNs, which makes it highly necessary but challenging to design effective and efficient QNNs.

In this paper, we formulate an analytical framework that correlates the structural properties of a single-qubit native QNN and its expressive power. We consider standard data re-uploading models that consist of interleaved data encoding circuit blocks and trainable circuit blocks. First, we prove that there exists a single-qubit native QNN that can express any Fourier series, which is a universal approximator for any square-integrable univariate function. It solves an open problem on the UAP of single-qubit QNNs in Ref. [27]. Second, we systematically analyze how parameters in trainable circuit blocks affect the Fourier coefficients. The main results on the expressivity of QNNs are summarized as in Fig. 1. We also provide numerical evidence on the approximation capabilities of QNN models. Third, we discuss potential difficulties for single-qubit native QNNs to approximate multivariate functions. Additionally, we compare native QNNs with the hybrid version and show the fundamental difference in their expressive power. We demonstrate the limitations of single-qubit native QNNs on approximating multivariate functions via numerical experiments. At last, we propose a possible strategy that extends single-qubit QNNs to multiple qubits, which could potentially overcome the limitations and handle practical classification tasks. Our analysis, beyond the UAP of QNNs, improves the understanding of the relationship between the expressive power and the structure of QNNs. This fundamental framework provides a theoretical foundation for data re-uploading QNN models, which is helpful to construct effective and efficient QNNs for quantum machine learning tasks.

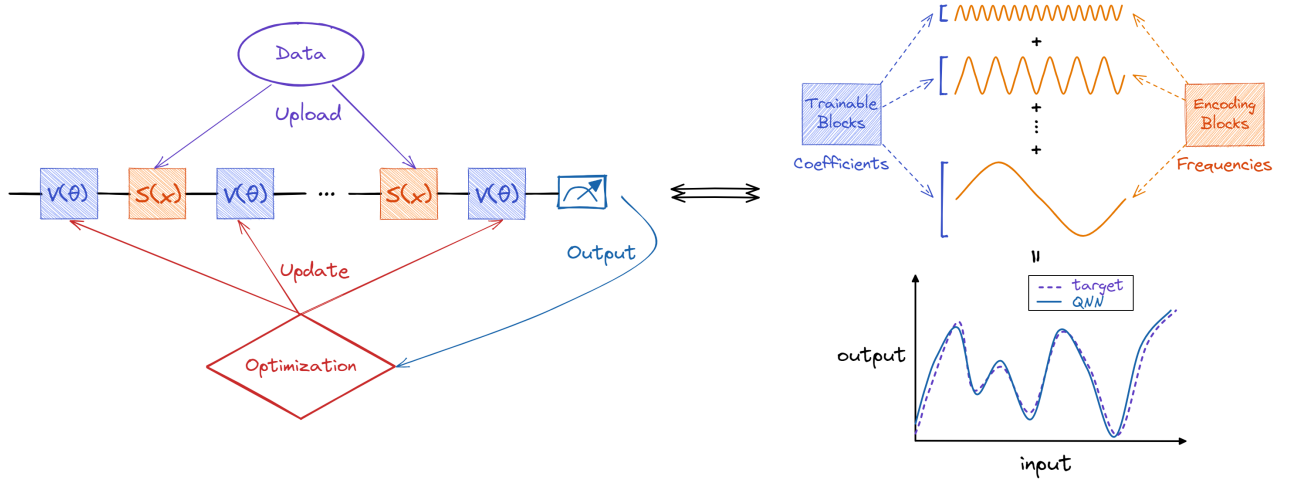


FIG. 1: **A schematic diagram of the main results.** A single-qubit data re-uploading QNN model consisting of interleaved trainable blocks (in blue) and encoding blocks (in orange) corresponds to a partial Fourier series. The encoding blocks decide the frequency spectrum of the Fourier series and the trainable blocks control the Fourier coefficients. By summability and convergence of the Fourier series, the QNN model can approximate any square-integrable target function.

We will start by giving some background and defining the native QNN models in the next section, and then analyze the expressivity of single-qubit native QNNs. In Section III, we discuss the limitation of single-qubit native QNNs and compare native QNNs with hybrid QNNs, which shows the fundamental difference

between their expressive power. The numerical experiments on the expressivity and limitations of single-qubit native QNNs are described in Section IV. An extension strategy to multi-qubit QNNs and their applications on classification tasks are presented in Section V.

II. EXPRESSIVITY OF SINGLE-QUBIT NATIVE QNN

We consider the data re-uploading QNN model [30], which is a generalized framework of quantum machine learning models based on parameterized quantum circuits [31]. A data re-uploading QNN is a quantum circuit that consists of interleaved data encoding circuit blocks $S(\cdot)$ and trainable circuit blocks $V(\cdot)$,

$$U_{\theta,L}(x) = V(\theta_0) \prod_{j=1}^L S(x)V(\theta_j), \quad (1)$$

where x is the input data, $\theta = (\theta_0, \dots, \theta_L)$ is a set of trainable parameters, and L denotes the number of layers of this model. We define the output of this model as the expectation value of measuring some observable M ,

$$f_{\theta,L}(x) = \langle 0 | U_{\theta,L}^\dagger(x) M U_{\theta,L}(x) | 0 \rangle. \quad (2)$$

Then the expressive power of $U_{\theta,L}(x)$ can be characterized by the classes of function that could be approximated by $f_{\theta,L}(x)$.

Note that some data re-uploading QNNs introduce trainable weights in data pre-processing or post-processing, which are considered as hybrid QNNs. For example, the data encoding block defined as $S(w \cdot x)$ is essentially equivalent to feeding data x into a neuron with weight w and then uploading the output to an encoding block $S(\cdot)$. Such a mixing structure makes it hard to tell whether the expressive power comes from the classical or quantum part. To solely study the expressive power of QNNs, we define the concept of *native QNN*, where all trainable weights are introduced by parameters of tunable quantum gates so that they can be distinguished from a hybrid QNN. Throughout this paper, we simply refer to the native QNN as QNN for short unless specified otherwise.

To better understand the expressive power of QNNs, we start our analysis from the simplest single-qubit QNNs. We consider the case of one-dimensional input data, i.e. $x \in \mathbb{R}$, which corresponds to the class of univariate functions. Ref. [27] investigated the expressive power of QNNs using the Fourier series formalism. The authors suggested that an L -layer QNN model can be expressed as truncated Fourier series of degree L and characterized the limits of the QNN model's expressivity by the richness of the frequency spectrum. However, the flexibility in the Fourier coefficient, which is a lot more difficult to analyze, remains less known. Thus the expressivity of single-qubit QNNs is still an open problem. In this section, we systematically investigate the correspondence between the single-qubit QNN and the partial Fourier sum in terms of both the frequency spectrum and Fourier coefficients, which solves this open problem.

A Fourier series is an expansion of a periodic function $f(x)$ in infinite terms of a sum of sines and cosines,

$$f(x) = \frac{a_0}{2} + \sum_{n=1}^{\infty} \left(a_n \cos\left(\frac{\pi}{T}nx\right) + b_n \sin\left(\frac{\pi}{T}nx\right) \right), \quad (3)$$

where Fourier coefficients are

$$a_0 = \frac{1}{T} \int_{-T}^T f(x) dx, \quad (4)$$

$$a_n = \frac{1}{T} \int_{-T}^T f(x) \cos\left(\frac{\pi}{T}nx\right) dx, \quad (5)$$

$$b_n = \frac{1}{T} \int_{-T}^T f(x) \sin\left(\frac{\pi}{T}nx\right) dx, \quad (6)$$

and T is half of the period of function $f(x)$. The quantities $n\frac{\pi}{T}$ are called the *frequencies*, which are multiples of the base frequency $\frac{\pi}{T}$. The set of frequency $\{n\frac{\pi}{T}\}_n$ is called the *frequency spectrum* of Fourier series. Applying Euler's formula, a Fourier series can be rewritten in the exponential form,

$$f(x) = \sum_{n=-\infty}^{\infty} c_n e^{i\frac{\pi}{T}nx}, \quad (7)$$

where $c_0 = \frac{1}{2}a_0$, $c_n = \frac{1}{2}(a_n + ib_n)$ for $n > 0$, and $c_n = \frac{1}{2}(a_n - ib_n)$ for $n < 0$. In approximation theory, a partial Fourier sum (or truncated Fourier series)

$$s_N(x) = \sum_{n=-N}^N c_n e^{i\frac{\pi}{T}nx} \quad (8)$$

is commonly used to approximate the function $f(x)$. A partial Fourier sum can be transformed to a Laurent polynomial $P \in \mathbb{C}[z, z^{-1}]$ by the substitution $z = e^{i\frac{\pi}{T}x}$, i.e.,

$$P(z) = \sum_{n=-N}^N c_n z^n. \quad (9)$$

A Laurent polynomial $P \in \mathbb{F}[z, z^{-1}]$ is a linear combination of positive and negative powers of the variable z with coefficients in \mathbb{F} . The *degree* of a Laurent polynomial P is the maximum absolute value of any exponent of z with non-zero coefficients, denoted by $\deg(P)$. We say that a Laurent polynomial P has parity 0 if all coefficients corresponding to odd powers of z are 0, and similarly P has parity 1 if all coefficients corresponding to even powers of z are 0.

Considering the data re-uploading QNNs defined in Eq. (1), it is natural to select the data encoding gate and trainable gate from the most prevalent parameterized quantum operators $\{R_X, R_Y, R_Z\}$. Following the pattern of Fourier series, we use $R_Z(x) = e^{-ixZ/2}$ to encode the input x and let $R_Y(\cdot)$ be the trainable gates. Then we can write the QNN as

$$U_{\theta,L}^{YZY}(x) = R_Y(\theta_0) \prod_{j=1}^L R_Z(x) R_Y(\theta_j), \quad (10)$$

and the quantum circuit is as follows:

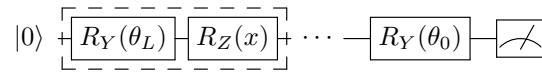


FIG. 2: The QNN model of L layers. Each layer consists of a trainable block and an encoding block, as shown in the dashed box. Here the trainable block is composed of Pauli rotation gates $R_Y(\cdot)$, while the encoding block is composed of Pauli rotation gate $R_Z(\cdot)$.

We show that the QNN $U_{\theta,L}^{YZY}(x)$ can be represented in the form of a partial Fourier sum with real coefficients.

Lemma 1 *There exists $\theta = (\theta_0, \theta_1, \dots, \theta_L) \in \mathbb{R}^{L+1}$ such that*

$$U_{\theta,L}^{YZY}(x) = \begin{bmatrix} P & -Q \\ Q^* & P^* \end{bmatrix} \quad (11)$$

if and only if real Laurent polynomials $P, Q \in \mathbb{R}[e^{ix/2}, e^{-ix/2}]$ satisfy

1. $\deg(P) = \deg(Q) \leq L$,
2. P and Q have parity $L \pmod{2}$,
3. $\forall x \in \mathbb{R}, |P|^2 + |Q|^2 = 1$.

Lemma 1 decomposes the unitary matrix of the QNN $U_{\theta,L}^{YZY}(x)$ into Laurent polynomials with real coefficients, which can be used to represent a partial Fourier sum with real coefficients. Note that the Fourier coefficients have a constraint $\sum_n |c_n| \leq 1$ by the condition 3 in Lemma 1.

The proof of Lemma 1 uses a method of mathematical induction that is in the similar spirit of the proof of quantum signal processing [32–34], which is a powerful subroutine in Hamiltonian simulation [4] and quantum singular value transformation [34]. The forward direction is straightforward by the definition of $U_{\theta,L}^{YZY}(x)$ in Eq. (10). The proof of the backward direction is by induction in L where the base case $L = 0$ holds trivially. For $L > 0$, we prove that for any $U_{\theta,L}^{YZY}(x)$ where P, Q satisfy the three conditions, there exists a unique block $R_Y^\dagger(\theta_k)R_Z^\dagger(x)$ such that polynomials \hat{P} and \hat{Q} in $U_{\theta,L}^{YZY}(x)R_Y^\dagger(\theta_k)R_Z^\dagger(x)$ satisfy the three conditions for $L - 1$. Lemma 1 explicitly correlates the frequency spectrum of the Fourier series and the number of layers L of the QNN. Note that the proof of Lemma 1 also illustrates the exact correspondence between the Fourier coefficients and parameters of trainable gates. A detailed proof can be found in Appendix I.

By Lemma 1, the partial Fourier sum corresponding to the QNN $U_{\theta,L}^{YZY}(x)$ only has real coefficients. With the exponential form of Eq. (7), a Fourier series with real coefficients only has $\cos(nx)$ terms, which means $U_{\theta,L}^{YZY}(x)$ can be used to approximate any even function on the interval $[-\pi, \pi]$. Thus we establish the following proposition, whose proof is deferred to Appendix II.

Proposition 2 *Let $|\psi(x)\rangle = U_{\theta,L}^{YZY}(x)|0\rangle$ and the observable be the Pauli Z operator. For any even square-integrable function $f : [-\pi, \pi] \rightarrow [-1, 1]$ and for all $\epsilon > 0$, there exist $L \in \mathbb{N}^+$ and $\theta \in \mathbb{R}^{L+1}$ such that*

$$\| \langle \psi(x) | Z | \psi(x) \rangle - f(x) \| \leq \epsilon. \quad (12)$$

Although the above result states that the QNN $U_{\theta,L}^{YZY}(x)|0\rangle$ is able to approximate a class of even functions within arbitrary precision, we can see that the main limitation of the expressive power of QNN $U_{\theta,L}^{YZY}(x)$ is the real Fourier coefficients, which may restrict its universal approximation capability.

To tackle this issue, our idea is to introduce complex coefficients to the corresponding Laurent polynomials, which can be implemented by adding a trainable Pauli Z rotation operator in each layer. Specifically, we consider the QNN

$$U_{\theta,\phi,L}^{WZW}(x) = W(\theta_0, \phi_0) \prod_{j=1}^L R_Z(x) W(\theta_j, \phi_j), \quad (13)$$

where each trainable block is $W(\theta_j, \phi_j) := R_Y(\theta_j)R_Z(\phi_j)$. The quantum circuit of $U_{\theta,\phi,L}^{WZW}(x)$ is as follows:

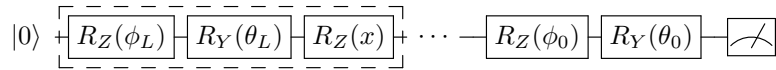


FIG. 3: The QNN model of L layers. Each layer consists of a trainable block and an encoding block, as shown in the dashed box. Here the trainable block is composed of Pauli rotation gates $R_Y(\cdot)$ and $R_Z(\cdot)$, while the encoding block is composed of Pauli rotation gate $R_Z(\cdot)$.

To characterize the capability of this QNN, we establish the following Lemma which implies $U_{\theta,\phi,L}^{WZW}(x)$ can express any Fourier partial sum with complex Fourier coefficients.

Lemma 3 *There exists $\theta = (\theta_0, \theta_1, \dots, \theta_L) \in \mathbb{R}^{L+1}$ and $\phi = (\phi_0, \phi_1, \dots, \phi_L) \in \mathbb{R}^{L+1}$ such that*

$$U_{\theta, \phi, L}^{\text{WZW}}(x) = \begin{bmatrix} P & -Q \\ Q^* & P^* \end{bmatrix} \quad (14)$$

if and only if Laurent polynomials $P, Q \in \mathbb{C}[e^{ix/2}, e^{-ix/2}]$ satisfy

1. $\deg(P) = \deg(Q) \leq L$,
2. P and Q have degree parity $L \pmod{2}$,
3. $\forall x \in \mathbb{R}, |P|^2 + |Q|^2 = 1$.

Lemma 3 demonstrates a decomposition of the QNN $U_{\theta, \phi, L}^{\text{WZW}}(x)$ into Laurent polynomials with complex coefficients, which can be used to represent a partial Fourier sum with complex coefficients in form of Eq. (8). The proof of Lemma 3 is also similar to the proof of Lemma 1 and its details are provided in Appendix III. Again, the proof demonstrates the effect of parameterized gates on the control of Fourier coefficients. We then prove in the following Theorem 4 that $U_{\theta, \phi, L}^{\text{WZW}}(x)$ is able to approximate any square-integrable function within arbitrary precision, using the well-established result in Fourier analysis. The detailed proof is deferred to Appendix IV.

Theorem 4 *Let $|\psi(x)\rangle = U_{\theta, \phi, L}^{\text{WZW}}(x) |0\rangle$ and the observable be the Pauli Z operator. For any square-integrable function $f : [-\pi, \pi] \rightarrow [-1, 1]$ and for all $\epsilon > 0$, there exist $L \in \mathbb{N}^+$ and $\theta \in \mathbb{R}^{L+1}, \phi \in \mathbb{R}^{L+1}$ such that*

$$\| \langle \psi(x) | Z | \psi(x) \rangle - f(x) \| \leq \epsilon. \quad (15)$$

Up till now we only let the encoding gate be the R_Z gate, what if we use other rotation operator gates to encode the data? It actually does not matter which one we choose as the encoding gate if the trainable gates are universal. Note that Pauli rotation operators $R_X(x), R_Y(x), R_Z(x)$ have two eigenvalues $\cos(x/2) \pm i \sin(x/2)$, and they can be diagonalized as $Q^\dagger R_Z(x) Q$. Merging unitaries Q^\dagger and Q to universal trainable gates gives the QNN that uses $R_Z(x)$ as the encoding gate. We hereby define the generic single-qubit QNNs as

$$U_{\theta, \phi, \lambda, L}^{\text{UZU}}(x) = U_3(\theta_0, \phi_0, \lambda_0) \prod_{j=1}^L R_Z(x) U_3(\theta_j, \phi_j, \lambda_j), \quad (16)$$

where each trainable block is the generic rotation gate

$$U_3(\theta, \phi, \lambda) = \begin{bmatrix} \cos \frac{\theta}{2} & -e^{i\lambda} \sin \frac{\theta}{2} \\ e^{i\phi} \sin \frac{\theta}{2} & e^{i(\phi+\lambda)} \cos \frac{\theta}{2} \end{bmatrix}. \quad (17)$$

By definition, any L -layer single-qubit QNN, including $U_{\theta, \phi, L}^{\text{WZW}}$, can be expressed as $U_{\theta, \phi, \lambda, L}^{\text{UZU}}$. Thus $U_{\theta, \phi, \lambda, L}^{\text{UZU}}$ is surely a universal approximator.

III. LIMITATIONS OF SINGLE-QUBIT NATIVE QNN

We have proved that a single-qubit QNN is a universal approximator for univariate functions, it is natural to consider its limitations. Is there a single-qubit QNN that can approximate arbitrary multivariate functions? We try to answer this question from the perspective of multivariate Fourier series. Specifically, we consider the

generic form of single-qubit QNNs defined in Eq. (16). For a d -dimensional data $\mathbf{x} := (x^{(1)}, x^{(2)}, \dots, x^{(d)}) \in \mathbb{R}^d$, let

$$U_{\boldsymbol{\theta}, L}(\mathbf{x}) = U_3(\theta_0, \phi_0, \lambda_0) \prod_{j=1}^L R_Z(x_j) U_3(\theta_j, \phi_j, \lambda_j), \quad (18)$$

where each $x_j \in \mathbf{x}$ and $L \in \mathbb{N}^+$. Further, let the output of the QNN be

$$f_{\boldsymbol{\theta}, L}(\mathbf{x}) = \langle 0 | U_{\boldsymbol{\theta}, L}^\dagger(\mathbf{x}) M U_{\boldsymbol{\theta}, L}(\mathbf{x}) | 0 \rangle \quad (19)$$

for an observable M . We write $V_j := U_3(\theta_j, \phi_j, \lambda_j)$ for short, that is

$$U_{\boldsymbol{\theta}, L}(\mathbf{x}) = V_0 \prod_{j=1}^L \begin{bmatrix} e^{-ix_j \lambda_0} & 0 \\ 0 & e^{-ix_j \lambda_1} \end{bmatrix} V_j, \quad (20)$$

where $\lambda_0 = \frac{1}{2}$ and $\lambda_1 = -\frac{1}{2}$. For the initial state $|0\rangle$, we have

$$U_{\boldsymbol{\theta}, L}(\mathbf{x}) |0\rangle = \sum_{j_1, \dots, j_L=0}^1 e^{-i(\lambda_{j_1} x_1 + \dots + \lambda_{j_L} x_L)} V_0 |j_1\rangle\langle j_1| V_1 \dots |j_L\rangle\langle j_L| V_L |0\rangle. \quad (21)$$

We denote I_i as the index set of encoding block $S(x^{(i)})$ and $I'_i = \{\lambda_{j_k} | k \in I_i\}$ for $i = 1, \dots, d$,

$$U_{\boldsymbol{\theta}, L}(\mathbf{x}) |0\rangle = \sum_{j \in \{0,1\}^L} e^{-i(\Lambda_j^{(1)} x^{(1)} + \dots + \Lambda_j^{(d)} x^{(d)})} V_0 |j_1\rangle\langle j_1| V_1 \dots |j_L\rangle\langle j_L| V_L |0\rangle, \quad (22)$$

where j is bit-strings composed of j_l , $l = 1, \dots, L$, and $\Lambda_j^{(i)} = \sum \lambda, \lambda \in I'_i$. Further,

$$f_{\boldsymbol{\theta}, L}(\mathbf{x}) = \sum_{j, \mathbf{k} \in \{0,1\}^L} C_{j, \mathbf{k}} e^{ih_{j, \mathbf{k}} \cdot \mathbf{x}}, \quad (23)$$

where

$$C_{j, \mathbf{k}} = \langle 0 | V_L^\dagger |k_L\rangle\langle k_L| V_{L-1}^\dagger \dots |k_1\rangle\langle k_1| V_1^\dagger M V_1 |j_1\rangle\langle j_1| \dots V_{L-1} |j_L\rangle\langle j_L| V_L |0\rangle, \quad (24)$$

and $h_{j, \mathbf{k}} = (\Lambda_{\mathbf{k}}^{(1)} - \Lambda_j^{(1)}, \dots, \Lambda_{\mathbf{k}}^{(d)} - \Lambda_j^{(d)})$. We consider the case of the i -th dimension,

$$\Lambda_{\mathbf{k}}^{(i)} - \Lambda_j^{(i)} = \{(\lambda_{k_1} + \dots + \lambda_{k_N}) - (\lambda_{j_1} + \dots + \lambda_{j_N}) | \lambda_{k_1} \dots \lambda_{k_N}, \lambda_{j_1} \dots \lambda_{j_N} \in I'_i\} \quad (25)$$

with $N = |I'_i|$. Since $\lambda_0 = \frac{1}{2}$ and $\lambda_1 = -\frac{1}{2}$, we can derive

$$\{\Lambda_{\mathbf{k}}^{(i)} - \Lambda_j^{(i)} | j, \mathbf{k} \in \{0,1\}^L\} = \{-N, \dots, 0, \dots, N\}. \quad (26)$$

Without loss of generality, we assume $|I'_i| = N$ for all $i = 1, \dots, d$. Then,

$$\{h_{j, \mathbf{k}} | j, \mathbf{k} \in \{0,1\}^L\} = \{-N, \dots, 0, \dots, N\}^d. \quad (27)$$

It can be inferred that a single-qubit QNN contains Fourier frequencies as rich as in Eq. (27). However, by the curse of dimensionality, it requires exponentially many terms in d to approximate a function in d dimensions. Thus a single-qubit QNN cannot match the flexibility of Fourier coefficients due to the constraint on degrees of freedom. Further, it implies that single-qubit QNNs may lack the capability to universally approximate arbitrary multivariate functions from the perspective of the Fourier series.

It has been proved that a single-qubit hybrid QNN can approximate arbitrary multivariate functions [28, 29]. However, the UAP of hybrid QNNs is fundamentally different from the native model that we investigated. Those hybrid models involve trainable weights either in data pre-processing or post-processing. Specifically, introducing trainable weights in data pre-processing is equivalent to multiplying each frequency of the Fourier series by an arbitrary real coefficient, i.e.

$$S(wx) = R_Z(wx) = e^{-iwx\frac{\pi}{2}Z}. \quad (28)$$

Therefore it enriches the frequency spectrum of native QNNs, which only contain integer multiples of the fundamental frequency. It can also be readily extended to the encoding of multi-dimensional data $\mathbf{x} := (x^{(1)}, x^{(2)}, \dots, x^{(d)})$ as

$$S(w_1x^{(1)})S(w_2x^{(2)}) \cdots S(w_dx^{(d)}) = R_Z(w_1x^{(1)})R_Z(w_2x^{(2)}) \cdots R_Z(w_dx^{(d)}) \quad (29)$$

$$= R_Z(\mathbf{w} \cdot \mathbf{x}) \quad (30)$$

$$= e^{-\frac{1}{2}i\mathbf{w} \cdot \mathbf{x}Z} \quad (31)$$

where $\mathbf{w} = (w_1, \dots, w_d)$ is a vector of trainable weights. Using such an encoding method enables a single-qubit QNN to approximate any continuous multivariate function [29]. We notice that, although the trainable weights enrich the frequency spectrum of the Fourier series, the capability of hybrid QNNs to approximate arbitrary multivariate functions is not obtained from the multivariate Fourier series, but from the universal approximation theorem [25, 26]. In another word, the expressivity of a hybrid QNN mostly comes from the classical structure, and the QNN serves as an activation function $\sigma(x) = e^{-ix}$ in the universal approximation theorem. This fact might be able to shed some light on the reason why a hybrid QNN does not provide quantum advantages over the classical NN.

IV. NUMERICAL EXPERIMENTS ON SINGLE-QUBIT QNN

In order to better illustrate the expressive power of single-qubit native QNNs, we supplement the theoretical results with numerical experiments. Specifically, we demonstrate the flexibility and approximation capability of single-qubit native QNNs in subsection IV A. The limitations of single-qubit QNNs are illustrated in subsection IV B through the numerical experiments on approximating multivariate functions. All simulations are carried out with the Paddle Quantum toolkit on the PaddlePaddle Deep Learning Platform [35].

A. Univariate function approximation

A damping function $f(x) = \frac{\sin(5x)}{5x}$ is used to demonstrate the approximation performance of single-qubit native QNN models of various number of layers. The dataset consists of 1000 data points uniformly sampled from the interval $[0, \pi]$, from which 200 are selected at random for the training set and 100 for the test set. Since the function $f(x) = \frac{\sin(5x)}{5x}$ is obviously an even function, we select the QNN model as defined in Eq. 10. The parameters of trainable gates are initialized from the uniform distribution on $[0, 2\pi]$. We adopt a variational quantum algorithm, where a gradient-based optimizer is used to search and update parameters in the QNN. Here the Adam optimizer is used with a learning rate of 0.1. We set the training iterations to be 100, with a batch size of 20 for all experiments.

While approximating a function $f(x)$ by a series expansion (e.g., Fourier series and Taylor series), the approximation error decreases gradually as the number of expansion terms increases. As shown in Lemma 3, the frequency spectrum and Fourier coefficients will be extended by consecutive repetitions of the encoding gate and trainable gate. The numerical results in Fig. 4 illustrate that the approximation error decreases as the number of layers increases, which is consistent with our theoretical analysis. Specifically, the QNN model

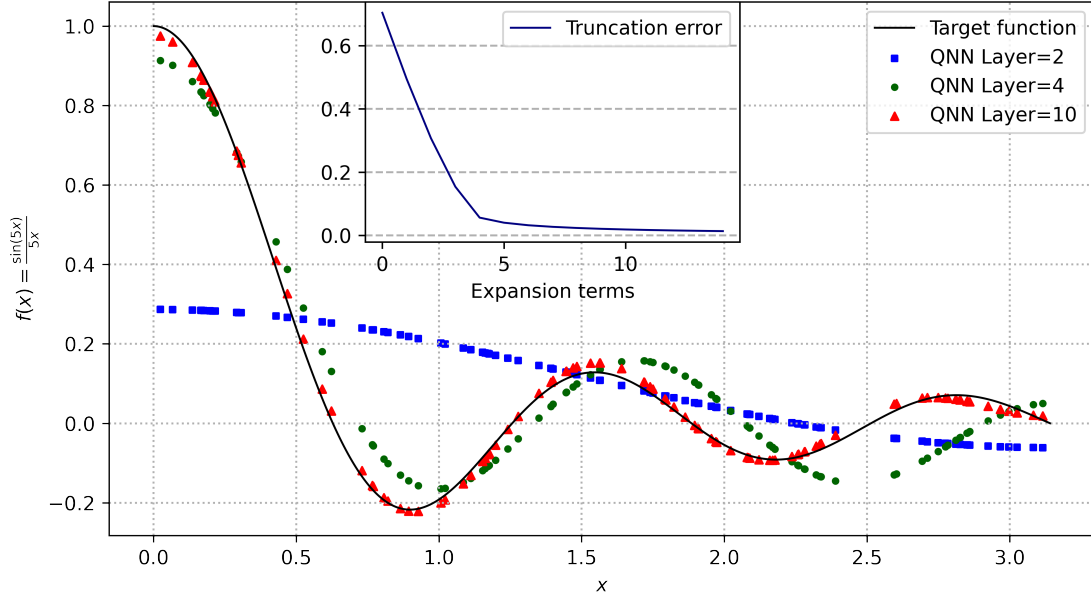


FIG. 4: Fitting the function $f(x) = \frac{\sin(5x)}{5x}$, $x \in [0, \pi]$ in $U_{\theta,L}^{ZZY}$ QNN with different number of layers. For the approximation, blue squares, green dots and red triangles indicate the simulation results of QNN with $L = 2$, $L = 4$ and $L = 10$, respectively. The theoretical truncation error is calculated using the uniform norm $\|f_N(x) - f(x)\|_\infty$, where $f_N(x)$ is the truncated Fourier series of $f(x)$ with N terms.

fails to fit the target function for $L = 2$ and $L = 4$. When L increases from 2 to 10, the predictions on test data become more accurate, i.e., the expressivity of the QNN model is decided by the number of layers L .

The Fourier series has a natural advantage in dealing with periodic functions. As stated previously, universal approximation theorems mainly focus on a bounded region, and the majority of models have satisfactory performances for learning the underlying function given proper data. In some cases, we may not only pay attention to interpolation but also explore the extrapolation behavior of the model. More explicitly, a class of functions with periodic nature will have the same pattern in an unbounded region. To further show the flexibility and capability of QNN, a fancy function, square wave, is selected to be the objective function.

The numerical results shown in Fig. 5 fully demonstrate the strength of the QNN model in dealing with periodic functions. By simply repeating 45 layers, the single-qubit QNN $U_{\theta,\phi,L}^{WZW}(x)$ learns the function hidden beneath the training data. More significantly, the approximation works well not only for input variables located between the training data but also outside of the region.

B. Multivariate function approximation

In this subsection, we numerically demonstrate the limitations of single-bit native QNNs in approximate multivariate functions. We examine the convergence of the loss as the number of layers of the circuit increases and compare the outcome with the target function. Specifically, we consider the bivariate function Himmelblau used in Ref. [29]. The 3D plot of the Himmelblau function is as shown in Fig. 6a.

Similarly, we first obtain data from the target function. The training set consists of 900 data points sampled from interval $[-\pi, \pi]^2$. We use the single-qubit QNN of various layers defined as Eq. (18) to learn the target function. The mean squared error (MSE) serves as the loss function. The experimental setting is the same as in the univariate function approximation, where a variational quantum algorithm is adopted.

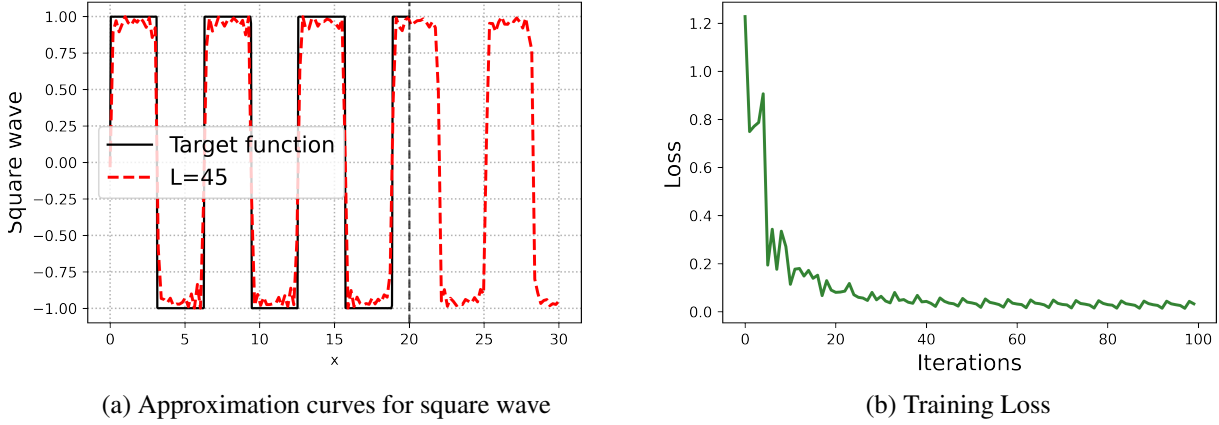


FIG. 5: Panel (a) shows the result of approximating square wave by a 45-layer QNN $U_{\theta, \phi, L}^{WZW}(x)$. Panel (b) is the loss during the training process. For showing periodic extrapolation, 400 data points are sampled uniformly from $[0, 20]$, and the test region is extend to $[0, 30]$.

The numerical results are shown in Fig. 6 imply that the single-qubit native QNN has difficulty in approximating bivariate functions. The approximation result of QNN as shown in Fig. 6b is quite different from the target Himmelblau function, even for a very deep circuit of 40 layers. Also, the training loss in Fig. 6c does not decrease as the number of layers increases. Note that the target function is only bivariate here, the limitations of single-qubit native QNNs will be more obvious in the case of higher dimensions.

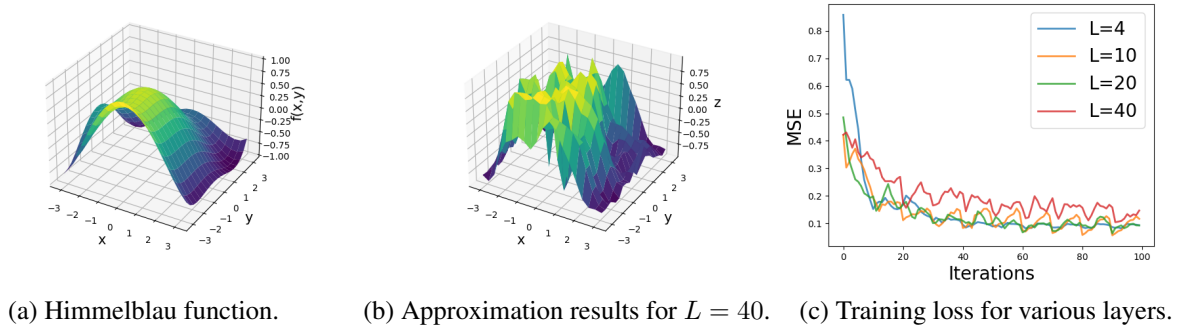


FIG. 6: Panel (a) is the target Himmelblau function $f(x, y) = (x^2 + y - 11)^2 + (x + y^2 - 7)^2$. Here $x, y \in [-\pi, \pi]$ and $f(x, y)$ is normalized, i.e., $-1 < f(x, y) < 1$. Panel (b) shows the approximation result of a 40-layer QNN. Panel (c) is the plot of training loss (MSE) during the optimization for different number of layers.

V. EXTENSION TO MULTI-QUBIT QNNS

We have already shown that the single-qubit native QNNs are able to approximate any univariate function but possibly could not approximate arbitrary multivariate functions by Fourier series. To address this limitation, research into the extension approach of single-qubit native QNNs is crucial. Analogous to classical NNs, they have significantly improved their capabilities from shallow to deep structures. We conjecture that QNNs have similar characteristics. We hereby provide an extension strategies as shown in Fig. 7, called *Parallel-Entanglement*. We introduce quantum entanglement by CNOT gates. Similar to classical NNs in

which different neurons are connected by trainable parameters to form deep NNs, QNNs can establish the connection between different qubits through quantum entanglement.

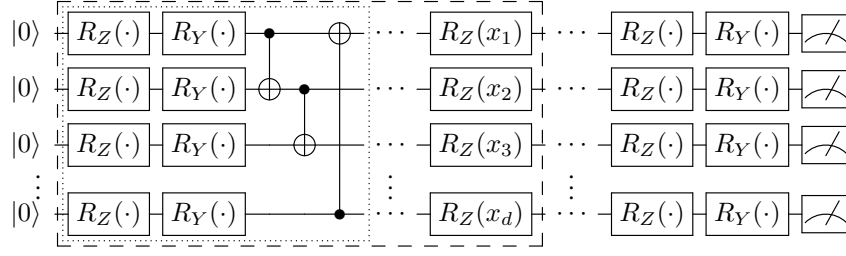


FIG. 7: The Parallel-Entanglement model with d qubits and L layers. Each layer consists of a trainable block and an encoding block, as shown in the dashed box. Here each trainable block is composed of repeated sub-blocks of Pauli rotation gates and CNOT gates, as shown in the dotted box. The number of sub-blocks in each trainable block is referred to as the *depth*. The encoding block is a tensor of Pauli rotation gate $R_Z(\cdot)$.

Through experiments on the classification task, we illustrate its potential to address practical problems. The public benchmark data sets are used to demonstrate the capabilities of Parallel-Entanglement models to tackle classification tasks. The results for classification tasks are summarized in Table I. The Iris data set contains 3

Dataset	Qubit	Layer	Depth	Parameter	Average Accuracy
Iris	4	1	1	16	0.990 ± 0.01
HTRU2	8	1	1	32	0.910 ± 0.09
		3	1	64	0.970 ± 0.03
		3	2	128	0.980 ± 0.02
Breast Cancer	4	1	1	16	0.780 ± 0.06
		3	1	32	0.840 ± 0.02
		3	2	64	0.845 ± 0.04

TABLE I: The performance of the Parallel-Entanglement model on Iris [36], Breast Cancer [37], and HTRU2 [38] data sets. Specifically, 100 pieces of data are sampled from the dataset, with 80% of them serving as the training set and 20% serving as the test set. With a learning rate of 0.1 and a batch size of 40, the Adam optimizer is still used to achieve the best results. To avoid the effects of initialization, we randomly ran the model 10 times, recording the average classification accuracy.

different classes, each class only has four attributes. Obviously, the 4-qubits model easily obtains an average accuracy of over 99% with only 1 layer on Iris data. The HTRU2 data set only has two categories, and each example has 8 attributes. As a result, an 8-qubit QNN is required to complete this task. The average accuracy for binary classification with 1 layer achieves above 91%. We can see that adding the number of layers to 3 and the depth of each layer to 2 increases the average accuracy to 98%. Since the Breast Cancer data contains 30 features for binary classification, the principal component analysis (PCA) is used to reduce feature dimension. Here the numerical results of a 4-qubit model are given to illustrate the power of the QNN. Compared to the model using complete information, the QNN model does not perform perfectly. But increasing the number of layers and the depth may improve the test accuracy. Based on the finding of the preceding experiments, it is clear that the Parallel-Entanglement model is capable of handling practical classification problems.

VI. CONCLUSION AND OUTLOOK

In this work, we presented a systematic investigation of the expressive power of single-qubit native QNNs, which are capable to approximate any square-integrable univariate function with arbitrary precision. We not

only give an existence proof but also analytically show an exact mapping between native QNNs and partial Fourier sums from perspectives of both frequency spectrum and Fourier coefficients, which solves an open problem on the UAP of single-qubit QNNs in Ref. [27]. Our proof, inspired by quantum signal processing, explicitly illustrates the correlation between parameters of trainable gates and the Fourier coefficients. Other than the expressivity, we also discuss the limitation of single-qubit QNNs from the perspective of multi-dimensional Fourier series. Both the expressivity and limitation of single-qubit QNNs are validated by numerical simulations. Other than the analysis of single-qubit QNNs, we also show the possibility of extending the QNNs to multiple qubits, which could potentially overcome the limitations of single-qubit QNNs and thus handle practical classification tasks. We expect our results provide a fundamental framework to the class of data re-uploading QNNs, which serves as insightful guidance on the design of such QNN models.

Although the expressive power and limitations of single-qubit QNNs have been well investigated, single-qubit models can be efficiently simulated by classical computers and hence cannot bring any quantum advantage. Therefore one future step is to generalize the framework of single-qubit QNNs to multivariate function approximators. The existence of multi-qubit QNNs that can approximate any multivariate functions has been proved in Ref. [27] under the assumption of exponential circuit depth and arbitrary observable, which are impractical to implement and also do not imply quantum advantage. A recent paper presents a method that extends quantum signal processing to multivariable [39], which might also be applicable to single-qubit QNNs. It is of great interest to study the optimal implementation of multi-qubit QNNs with multivariate universal approximation properties, which may potentially offer computational advantages over classical techniques.

Acknowledgements. We would like to thank Runyao Duan for helpful suggestions on quantum signal processing. We also thank Guangxi Li, Geng Liu, Youle Wang, Haokai Zhang, Lei Zhang, and Chengkai Zhu for useful comments. Z. Y., H. Y., and M. L. contributed equally to this work. Part of this work was done when Z. Y., H. Y., and M. L. were research interns at Baidu Research.

-
- [1] Peter W. Shor. Polynomial-Time Algorithms for Prime Factorization and Discrete Logarithms on a Quantum Computer. *SIAM Journal on Computing*, 26(5):1484–1509, oct 1997.
 - [2] Lov K Grover. A fast quantum mechanical algorithm for database search. In *Proceedings of the twenty-eighth annual ACM symposium on Theory of computing - STOC '96*, pages 212–219, New York, New York, USA, 1996. ACM Press.
 - [3] Seth Lloyd. Universal Quantum Simulators. *Science*, 273(5278):1073–1078, aug 1996.
 - [4] Andrew M. Childs, Dmitri Maslov, Yunseong Nam, Neil J. Ross, and Yuan Su. Toward the first quantum simulation with quantum speedup. *Proceedings of the National Academy of Sciences*, 115(38):9456–9461, sep 2018.
 - [5] Frank Arute, Kunal Arya, Ryan Babbush, Dave Bacon, Joseph C Bardin, Rami Barends, Rupak Biswas, Sergio Boixo, Fernando GSL Brandao, David A Buell, et al. Quantum supremacy using a programmable superconducting processor. *Nature*, 574(7779):505–510, 2019.
 - [6] Yulin Wu, Wan-Su Bao, Sirui Cao, Fusheng Chen, Ming-Cheng Chen, Xiawei Chen, Tung-Hsun Chung, Hui Deng, Yajie Du, Daojin Fan, Ming Gong, Cheng Guo, Chu Guo, Shaojun Guo, Lianchen Han, Linyin Hong, He-Liang Huang, Yong-Heng Huo, Liping Li, Na Li, Shaowei Li, Yuan Li, Futian Liang, Chun Lin, Jin Lin, Haoran Qian, Dan Qiao, Hao Rong, Hong Su, Lihua Sun, Liangyuan Wang, Shiyu Wang, Dachao Wu, Yu Xu, Kai Yan, Weifeng Yang, Yang Yang, Yangsen Ye, Jianghan Yin, Chong Ying, Jiale Yu, Chen Zha, Cha Zhang, Haibin Zhang, Kaili Zhang, Yiming Zhang, Han Zhao, Youwei Zhao, Liang Zhou, Qingling Zhu, Chao-Yang Lu, Cheng-Zhi Peng, Xiaobo Zhu, and Jian-Wei Pan. Strong Quantum Computational Advantage Using a Superconducting Quantum Processor. *Physical Review Letters*, 127(18):180501, oct 2021.
 - [7] Han-Sen Zhong, Hui Wang, Yu-Hao Deng, Ming-Cheng Chen, Li-Chao Peng, Yi-Han Luo, Jian Qin, Dian Wu, Xing Ding, Yi Hu, Peng Hu, Xiao-Yan Yang, Wei-Jun Zhang, Hao Li, Yuxuan Li, Xiao Jiang, Lin Gan, Guangwen Yang, Lixing You, Zhen Wang, Li Li, Nai-Le Liu, Chao-Yang Lu, and Jian-Wei Pan. Quantum computational advantage using photons. *Science*, 370(6523):1460–1463, dec 2020.
 - [8] Jacob Biamonte, Peter Wittek, Nicola Pancotti, Patrick Rebentrost, Nathan Wiebe, and Seth Lloyd. Quantum machine learning. *Nature*, 549(7671):195–202, sep 2017.
 - [9] M. Cerezo, Andrew Arrasmith, Ryan Babbush, Simon C. Benjamin, Suguru Endo, Keisuke Fujii, Jarrod R. Mc-

- Clean, Kosuke Mitarai, Xiao Yuan, Lukasz Cincio, and Patrick J. Coles. Variational quantum algorithms. *Nature Reviews Physics*, aug 2021.
- [10] Kishor Bharti, Alba Cervera-Lierta, Thi Ha Kyaw, Tobias Haug, Sumner Alperin-Lea, Abhinav Anand, Matthias Degroote, Hermann Heimonen, Jakob S Kottmann, Tim Menke, Wai-Keong Mok, Sukin Sim, Leong-Chuan Kwek, and Alán Aspuru-Guzik. Noisy intermediate-scale quantum (NISQ) algorithms. *arXiv:2101.08448*, pages 1–82, jan 2021.
 - [11] Suguru Endo, Zhenyu Cai, Simon C Benjamin, and Xiao Yuan. Hybrid Quantum-Classical Algorithms and Quantum Error Mitigation. *Journal of the Physical Society of Japan*, 90(3):032001, mar 2021.
 - [12] Jonathan Romero, Jonathan P. Olson, and Alan Aspuru-Guzik. Quantum autoencoders for efficient compression of quantum data. *Quantum Science and Technology*, 2(4):045001, dec 2017.
 - [13] Chenfeng Cao and Xin Wang. Noise-Assisted Quantum Autoencoder. *Physical Review Applied*, 15(5):054012, may 2021.
 - [14] Iris Cong, Soonwon Choi, and Mikhail D. Lukin. Quantum convolutional neural networks. *Nature Physics*, 15(12):1273–1278, dec 2019.
 - [15] Weikang Li and Dong-Ling Deng. Recent advances for quantum classifiers. *arXiv:2108.13421*, aug 2021.
 - [16] Maria Schuld and Francesco Petruccione. *Machine Learning with Quantum Computers*. Springer, 2021.
 - [17] G. Li, Z. Song, and X. Wang. VSQ: Variational shadow quantum learning for classification. In *Proceedings of the AAAI Conference on Artificial Intelligence*, 35(9), 8357–8365, 2021.
 - [18] Sumeet Khatri, Ryan LaRose, Alexander Poremba, Lukasz Cincio, Andrew T. Sornborger, and Patrick J. Coles. Quantum-assisted quantum compiling. *Quantum*, 3:140, jul 2018.
 - [19] Zhan Yu, Xuanqiang Zhao, Benchu Zhao, and Xin Wang. Optimal quantum dataset for learning a unitary transformation. *arXiv preprint arXiv:2203.00546*, mar 2022.
 - [20] Matthias C Caro, Hsin-Yuan Huang, Nicholas Ezzell, Joe Gibbs, Andrew T Sornborger, Lukasz Cincio, Patrick J Coles, and Zoë Holmes. Out-of-distribution generalization for learning quantum dynamics. *arXiv preprint arXiv:2204.10268*, apr 2022.
 - [21] Sam McArdle, Suguru Endo, Alán Aspuru-Guzik, Simon C. Benjamin, and Xiao Yuan. Quantum computational chemistry. *Reviews of Modern Physics*, 92(1):015003, mar 2020.
 - [22] Bálint Koczor, Suguru Endo, Tyson Jones, Yuichiro Matsuzaki, and Simon C Benjamin. Variational-state quantum metrology. *New Journal of Physics*, 22(8):083038, aug 2020.
 - [23] Jacob L. Beckey, M. Cerezo, Akira Sone, and Patrick J. Coles. Variational quantum algorithm for estimating the quantum Fisher information. *Physical Review Research*, 4(1):013083, feb 2022.
 - [24] Johannes Jakob Meyer, Johannes Borregaard, and Jens Eisert. A variational toolbox for quantum multi-parameter estimation. *npj Quantum Information*, 7(1):89, dec 2021.
 - [25] George Cybenko. Approximation by superpositions of a sigmoidal function. *Mathematics of control, signals and systems*, 2(4):303–314, 1989.
 - [26] Kurt Hornik. Approximation capabilities of multilayer feedforward networks. *Neural networks*, 4(2):251–257, 1991.
 - [27] Maria Schuld, Ryan Sweke, and Johannes Jakob Meyer. Effect of data encoding on the expressive power of variational quantum-machine-learning models. *Physical Review A*, 103(3):032430, 2021.
 - [28] Takahiro Goto, Quoc Hoan Tran, and Kohei Nakajima. Universal approximation property of quantum machine learning models in quantum-enhanced feature spaces. *Physical Review Letters*, 127(9):090506, 2021.
 - [29] Adrián Pérez-Salinas, David López-Núñez, Artur García-Sáez, Pol Forn-Díaz, and José I Latorre. One qubit as a universal approximant. *Physical Review A*, 104(1):012405, 2021.
 - [30] Adrián Pérez-Salinas, Alba Cervera-Lierta, Elies Gil-Fuster, and José I. Latorre. Data re-uploading for a universal quantum classifier. *Quantum*, 4:226, February 2020.
 - [31] Sofiene Jerbi, Lukas J. Fiderer, Hendrik Poulsen Nautrup, Jonas M. Kübler, Hans J. Briegel, and Vedran Dunjko. Quantum machine learning beyond kernel methods. *arXiv:2110.13162 [quant-ph, stat]*, February 2022.
 - [32] Guang Hao Low and Isaac L. Chuang. Optimal hamiltonian simulation by quantum signal processing. *Physical Review Letters*, 118(1):010501, January 2017.
 - [33] Jeongwan Haah. Product decomposition of periodic functions in quantum signal processing. *Quantum*, 3:190, October 2019.
 - [34] András Gilyén, Yuan Su, Guang Hao Low, and Nathan Wiebe. Quantum singular value transformation and beyond: Exponential improvements for quantum matrix arithmetics. *Proceedings of the 51st Annual ACM SIGACT Symposium on Theory of Computing*, pages 193–204, June 2019.
 - [35] Yanjun Ma, Dianhai Yu, Tian Wu, and Haifeng Wang. Paddlepaddle: An open-source deep learning platform from industrial practice. *Frontiers of Data and Computing*, 1(1):105–115, 2019.

- [36] Ronald A Fisher. The use of multiple measurements in taxonomic problems. *Annals of eugenics*, 7(2):179–188, 1936.
- [37] Ryszard S Michalski, Igor Mozetic, Jiarong Hong, and Nada Lavrac. The multi-purpose incremental learning system aq15 and its testing application to three medical domains. In *Proc. AAAI*, volume 1986, pages 1–041, 1986.
- [38] Robert J Lyon, BW Stappers, Sally Cooper, John Martin Brooke, and Joshua D Knowles. Fifty years of pulsar candidate selection: from simple filters to a new principled real-time classification approach. *Monthly Notices of the Royal Astronomical Society*, 459(1):1104–1123, 2016.
- [39] Zane M. Rossi and Isaac L. Chuang. Multivariable quantum signal processing (m-qsp): prophecies of the two-headed oracle, 2022.
- [40] Ferenc Weisz. Summability of multi-dimensional trigonometric fourier series. *arXiv preprint arXiv:1206.1789*, 2012.

Appendix for Power and limitations of single-qubit native quantum neural networks

I. PROOF OF LEMMA 1

Lemma 1 *There exists $\theta = (\theta_0, \theta_1, \dots, \theta_L) \in \mathbb{R}^{L+1}$ such that*

$$U_{\theta, L}^{YZY}(x) = \begin{bmatrix} P & -Q \\ Q^* & P^* \end{bmatrix} \quad (\text{S1})$$

if and only if real Laurent polynomials $P, Q \in \mathbb{R}[e^{ix/2}, e^{-ix/2}]$ satisfy

1. $\deg(P) = \deg(Q) \leq L$,
2. P and Q have parity $L \pmod{2}$,
3. $\forall x \in \mathbb{R}, |P|^2 + |Q|^2 = 1$.

Proof First we prove the forward direction, i.e. Eq. (S1) implies the three conditions, by induction on L . For the base case, if $L = 0$, then $R_Y(\theta_0)$ gives $P = \cos(\theta_0/2)$ and $Q = \sin(\theta_0/2)$, which clearly satisfies the conditions.

For the induction step, suppose Eq. (S1) satisfies the three conditions. Then

$$\begin{bmatrix} P & -Q \\ Q^* & P^* \end{bmatrix} R_Z(x) R_Y(\theta_k) \quad (\text{S2})$$

$$= \begin{bmatrix} P & -Q \\ Q^* & P^* \end{bmatrix} \begin{bmatrix} \cos(\theta_k/2)e^{-ix/2} & -\sin(\theta_k/2)e^{-ix/2} \\ \sin(\theta_k/2)e^{ix/2} & \cos(\theta_k/2)e^{ix/2} \end{bmatrix} \quad (\text{S3})$$

$$= \begin{bmatrix} \cos \frac{\theta_k}{2} e^{-ix/2} P - \sin \frac{\theta_k}{2} e^{ix/2} Q & -\sin \frac{\theta_k}{2} e^{-ix/2} P - \cos \frac{\theta_k}{2} e^{ix/2} Q \\ \cos \frac{\theta_k}{2} e^{-ix/2} Q^* + \sin \frac{\theta_k}{2} e^{ix/2} P^* & \cos \frac{\theta_k}{2} e^{ix/2} P^* - \sin \frac{\theta_k}{2} e^{-ix/2} Q^* \end{bmatrix} \quad (\text{S4})$$

$$= \begin{bmatrix} \bar{P} & -\bar{Q} \\ \bar{Q}^* & \bar{P}^* \end{bmatrix} \quad (\text{S5})$$

where

$$\bar{P} = \cos \frac{\theta_k}{2} e^{-ix/2} P - \sin \frac{\theta_k}{2} e^{ix/2} Q, \quad (\text{S6})$$

$$\bar{Q} = \sin \frac{\theta_k}{2} e^{-ix/2} P + \cos \frac{\theta_k}{2} e^{ix/2} Q \quad (\text{S7})$$

clearly satisfy the first condition $\deg(\bar{P}) = \deg(\bar{Q}) \leq L + 1$. They also satisfy the second condition since multiplying by $e^{-ix/2}$ or $e^{ix/2}$ alters the degree parity. The third condition follows from unitarity.

Next we show the reverse by induction on L that the three conditions suffice to construct the QNN in Eq. (S1). For the base case, we have $L = 0$ and $\deg(P) = \deg(Q) = 0$. Note that P and Q are real polynomials, i.e. the coefficients must be real numbers, so condition 3 implies that $P = \cos(\theta_0/2)$ and $Q = \sin(\theta_0/2)$ for some $\theta_0 \in \mathbb{R}$. Thus the matrix

$$\begin{bmatrix} P & -Q \\ Q^* & P^* \end{bmatrix} \quad (\text{S8})$$

can be written as a QNN $U_{\theta,0}^{YZY}(x) = R_Y(\theta_0)$.

For the induction step, suppose Laurent polynomials P and Q satisfy the three conditions for some $L > 0$. We first observe that condition 3 implies

$$|P|^2 + |Q|^2 = PP^* + QQ^* = 1, \quad (\text{S9})$$

where $PP^* + QQ^*$ is a Laurent polynomial with parity $2n \pmod{2} \equiv 0$. Let $d := \deg(P) = \deg(Q)$, then $d \leq L$ by the first condition. Since Eq. (S9) holds for all $x \in \mathbb{R}$, the leading coefficients must satisfy $p_d p_{-d} + q_d q_{-d} = 0$ so they cancel. We choose $\theta_k \in \mathbb{R}$ so that

$$\cos \frac{\theta_k}{2} p_d + \sin \frac{\theta_k}{2} q_d = 0, \quad (\text{S10})$$

$$-\sin \frac{\theta_k}{2} p_{-d} + \cos \frac{\theta_k}{2} q_{-d} = 0. \quad (\text{S11})$$

Now we briefly argue that there always exists a θ_k satisfies equations above. If all p_d, p_{-d}, q_d, q_{-d} are not 0, simply let $\tan \frac{\theta_k}{2} = -\frac{p_d}{q_d}$. Then consider the case of zero coefficients. Since $\deg(P) = \deg(Q) = d$, at most two of p_d, p_{-d}, q_d, q_{-d} could be 0. The fact $p_d p_{-d} + q_d q_{-d} = 0$ implies that one of p_d, p_{-d} is 0 if and only if one of q_d, q_{-d} is 0. If $p_d = q_d = 0$ (or $p_{-d} = q_{-d} = 0$), pick θ_k so that $\tan \frac{\theta_k}{2} = \frac{q_{-d}}{p_{-d}}$ (or $\tan \frac{\theta_k}{2} = -\frac{p_d}{q_d}$). If $p_d = q_{-d} = 0$ (or $p_{-d} = q_d = 0$), pick θ_k so that $\sin \frac{\theta_k}{2} = 0$ (or $\cos \frac{\theta_k}{2} = 0$).

Next, for the θ_k that satisfies Eq. (S10) and Eq. (S11) simultaneously, we consider

$$\begin{bmatrix} P & -Q \\ Q^* & P^* \end{bmatrix} R_Y^\dagger(\theta_k) R_Z^\dagger(x) \quad (\text{S12})$$

$$= \begin{bmatrix} \cos \frac{\theta_k}{2} e^{ix/2} P + \sin \frac{\theta_k}{2} e^{ix/2} Q & -\cos \frac{\theta_k}{2} e^{-ix/2} Q + \sin \frac{\theta_k}{2} e^{-ix/2} P \\ \cos \frac{\theta_k}{2} e^{ix/2} Q^* - \sin \frac{\theta_k}{2} e^{ix/2} P^* & \cos \frac{\theta_k}{2} e^{-ix/2} P^* + \sin \frac{\theta_k}{2} e^{-ix/2} Q \end{bmatrix} \quad (\text{S13})$$

$$= \begin{bmatrix} \hat{P} & -\hat{Q} \\ \hat{Q}^* & \hat{P}^* \end{bmatrix} \quad (\text{S14})$$

where

$$\hat{P} = \cos \frac{\theta_k}{2} e^{ix/2} P + \sin \frac{\theta_k}{2} e^{ix/2} Q, \quad (\text{S15})$$

$$\hat{Q} = \cos \frac{\theta_k}{2} e^{-ix/2} Q - \sin \frac{\theta_k}{2} e^{-ix/2} P. \quad (\text{S16})$$

Since $P, Q \in \mathbb{R}[e^{ix/2}, e^{-ix/2}]$ are Laurent polynomials with degree d , $\hat{P} \in \mathbb{R}[e^{ix/2}, e^{-ix/2}]$ might appear to be a Laurent polynomial with degree $d + 1$. In fact it has degree $\deg(\hat{P}) \leq d - 1$, because the coefficient of $(e^{ix/2})^{d+1}$ term in \hat{P} is $\cos \frac{\theta_k}{2} p_d + \sin \frac{\theta_k}{2} q_d = 0$ by the choice of θ_k , and the coefficient of $(e^{ix/2})^d$ term is 0 by condition 2. Similarly, \hat{Q} has leading coefficient $\cos \frac{\theta_k}{2} q_{-d} - \sin \frac{\theta_k}{2} p_{-d} = 0$ and has degree $\deg(\hat{Q}) \leq d - 1$.

Since $d \leq L$, we have $\deg(\hat{P}) = \deg(\hat{Q}) \leq L - 1$, hence condition 1 is satisfied. From the degree parity of P and Q , it is easy to see that \hat{P} and \hat{Q} have degree parity $L - 1 \pmod{2}$, thus condition 2 is satisfied. Condition 3 follows from unitarity. By the induction hypothesis, Eq. (S14) can be written as a QNN in the form of $U_{\theta, L-1}^{YZY}(x)$, and therefore the matrix

$$\begin{bmatrix} P & -Q \\ Q^* & P^* \end{bmatrix} \quad (\text{S17})$$

can be written as a QNN in the form of $U_{\theta, L}^{YZY}(x)$. ■

We note that the above proof is in a similar spirit of the proof of quantum signal processing [32–34].

II. PROOF OF PROPOSITION 2

Proposition 2 *Let $|\psi(x)\rangle = U_{\theta, L}^{YZY}(x) |0\rangle$ and the observable be the Pauli Z operator. For any even square-integrable function $f : [-\pi, \pi] \rightarrow [-1, 1]$ and for all $\epsilon > 0$, there exist $L \in \mathbb{N}^+$ and $\theta \in \mathbb{R}^{L+1}$ such that*

$$\| \langle \psi(x) | Z | \psi(x) \rangle - f(x) \| \leq \epsilon. \quad (\text{S18})$$

Proof First, it is known that any even square-integrable function $f(x)$ can be approximated by a truncated Fourier series [40]. For any $\epsilon > 0$, there exists a $K \in \mathbb{N}^+$ such that

$$\| f_K(x) - f(x) \| \leq \frac{\epsilon}{2}, \quad (\text{S19})$$

where $f_K(x)$ is the K -term partial Fourier sum of even function $f(x)$. Consider the function $\sqrt{\frac{1+f_K(x)}{2}}$, using the property of square-integrable functions again, there exists an $L \in \mathbb{N}^+$ such that

$$\left\| g_L(x) - \sqrt{\frac{1+f_K(x)}{2}} \right\| \leq \frac{\epsilon}{8}, \quad (\text{S20})$$

where

$$g_L(x) = a_0 + \sum_{n=1}^{L/2} a_n \cos(nx) \quad (\text{S21})$$

is the partial Fourier sum of the even function $\sqrt{\frac{1+f_K(x)}{2}}$ and $L \pmod{2} = 0$. Next we need to prove

$$\langle 0 | U_{\theta, L}^{YZY}(x) | 0 \rangle = g_L(x). \quad (\text{S22})$$

Specifically, $g_L(x)$ can be written as follows,

$$g_L(x) = \sum_{n=-L/2}^{L/2} c_n e^{inx} = \sum_{n=-L/2}^{L/2} c_n (e^{ix/2})^{2n}, \quad (\text{S23})$$

where $c_n = c_{-n} = a_n/2$. Obviously, $g_L \in \mathbb{R}[e^{ix/2}, e^{-ix/2}]$ and conditions of Lemma 1 are satisfied, so Eq. (S22) holds. Further, we have

$$\| \langle \psi(x) | Z | \psi(x) \rangle - f_K(x) \| = 2 \left\| g_L^2(x) - \frac{1+f_K(x)}{2} \right\|, \quad (\text{S24})$$

$$\leq 4 \left\| g_L(x) - \sqrt{\frac{1+f_K(x)}{2}} \right\|, \quad (\text{S25})$$

$$\leq \frac{\epsilon}{2}, \quad (\text{S26})$$

where $\|g_L(x)\| \leq 1$ and $\left\| \sqrt{\frac{1+f_K(x)}{2}} \right\| \leq 1$. Finally, combined with inequality (S19), inequality (S18) holds. \blacksquare

III. PROOF OF LEMMA 3

Lemma 3 *There exists $\theta = (\theta_0, \theta_1, \dots, \theta_L) \in \mathbb{R}^{L+1}$ and $\phi = (\phi_0, \phi_1, \dots, \phi_L) \in \mathbb{R}^{L+1}$ such that*

$$U_{\theta, \phi, L}^{\text{WZW}}(x) = \begin{bmatrix} P & -Q \\ Q^* & P^* \end{bmatrix} \quad (\text{S27})$$

if and only if Laurent polynomials $P, Q \in \mathbb{C}[e^{ix/2}, e^{-ix/2}]$ satisfy

1. $\deg(P) = \deg(Q) \leq L$,
2. P and Q have degree parity $L \pmod{2}$,
3. $\forall x \in \mathbb{R}, |P|^2 + |Q|^2 = 1$.

Proof The entire proof is similar as the proof of Lemma 1, and the only difference is that the coefficients of Laurent polynomials could be complex rather than real. First we prove the forward direction by induction on L . For the base case, if $L = 0$, then $W(\theta_0, \phi_0) = R_Y(\theta_0)R_Z(\phi_0)$ gives $P = e^{-i\frac{\phi_0}{2}} \cos(\theta_0/2)$ and $Q = e^{i\frac{\phi_0}{2}} \sin(\theta_0/2)$, which clearly satisfies the three conditions.

For the induction step, suppose Eq. (S27) satisfies the three conditions. Then

$$\begin{bmatrix} P & -Q \\ Q^* & P^* \end{bmatrix} R_Z(x) R_Y(\theta_k) R_Z(\phi_k) \quad (\text{S28})$$

$$= \begin{bmatrix} P & -Q \\ Q^* & P^* \end{bmatrix} \begin{bmatrix} \cos \frac{\theta_k}{2} e^{-i\frac{\phi_k}{2}} e^{-i\frac{x}{2}} & -\sin \frac{\theta_k}{2} e^{i\frac{\phi_k}{2}} e^{-i\frac{x}{2}} \\ \sin \frac{\theta_k}{2} e^{-i\frac{\phi_k}{2}} e^{i\frac{x}{2}} & \cos \frac{\theta_k}{2} e^{i\frac{\phi_k}{2}} e^{i\frac{x}{2}} \end{bmatrix} \quad (\text{S29})$$

$$= \begin{bmatrix} \cos \frac{\theta_k}{2} e^{-i\frac{\phi_k}{2}} e^{-i\frac{x}{2}} P - \sin \frac{\theta_k}{2} e^{-i\frac{\phi_k}{2}} e^{i\frac{x}{2}} Q & -\sin \frac{\theta_k}{2} e^{i\frac{\phi_k}{2}} e^{-i\frac{x}{2}} P - \cos \frac{\theta_k}{2} e^{i\frac{\phi_k}{2}} e^{i\frac{x}{2}} Q \\ \cos \frac{\theta_k}{2} e^{-i\frac{\phi_k}{2}} e^{-i\frac{x}{2}} Q^* + \sin \frac{\theta_k}{2} e^{-i\frac{\phi_k}{2}} e^{i\frac{x}{2}} P^* & \cos \frac{\theta_k}{2} e^{i\frac{\phi_k}{2}} e^{i\frac{x}{2}} P^* - \sin \frac{\theta_k}{2} e^{i\frac{\phi_k}{2}} e^{-i\frac{x}{2}} Q^* \end{bmatrix} \quad (\text{S30})$$

$$= \begin{bmatrix} \bar{P} & -\bar{Q} \\ \bar{Q}^* & \bar{P}^* \end{bmatrix} \quad (\text{S31})$$

where

$$\bar{P} = \cos \frac{\theta_k}{2} e^{-i\frac{\phi_k}{2}} e^{-i\frac{x}{2}} P - \sin \frac{\theta_k}{2} e^{-i\frac{\phi_k}{2}} e^{i\frac{x}{2}} Q, \quad (\text{S32})$$

$$\bar{Q} = \sin \frac{\theta_k}{2} e^{i\frac{\phi_k}{2}} e^{-i\frac{x}{2}} P + \cos \frac{\theta_k}{2} e^{i\frac{\phi_k}{2}} e^{i\frac{x}{2}} Q \quad (\text{S33})$$

clearly satisfy the first condition $\deg(\bar{P}) = \deg(\bar{Q}) \leq L + 1$. They also satisfy the second condition since multiplying by $e^{-ix/2}$ or $e^{ix/2}$ alters the degree parity. The third condition is satisfied because of unitarity.

Next we show the backward direction by induction on L that the three conditions suffice to construct the QNN in Eq. (S27). First we consider the base case of $L = 0$, we have $\deg(P) = \deg(Q) = 0$, the above condition implies that $P = e^{-i\phi_0/2} \cos(\theta_0/2)$ and $Q = e^{i\phi_0/2} \sin(\theta_0/2)$ for some $\theta_0, \phi_0 \in \mathbb{R}$. Thus the matrix

$$\begin{bmatrix} P & -Q \\ Q^* & P^* \end{bmatrix} \quad (\text{S34})$$

can be written as a QNN $U_{\theta, \phi, L}^{\text{WZW}}(x) = R_Y(\theta_0)R_Z(\phi_0)$.

For the induction step, suppose Laurent polynomials P and Q satisfy the three conditions for some $L > 0$. We first observe that condition 3 implies

$$|P|^2 + |Q|^2 = PP^* + QQ^* = 1, \quad (\text{S35})$$

where $PP^* + QQ^*$ is a polynomial in $e^{ix/2}$ with parity $2n \pmod{2} = 0$. Since Eq. (S35) holds for all $x \in \mathbb{R}$, the leading coefficients must satisfy $p_d p_{-d}^* + q_d q_{-d}^* = 0$ and $p_d^* p_{-d} + q_d^* q_{-d} = 0$, where $d := \deg(P) = \deg(Q)$. By the first condition, we have $d \leq L$. We choose $\theta_k, \phi_k \in \mathbb{R}$ so that

$$\cos \frac{\theta_k}{2} e^{i\frac{\phi_k}{2}} p_d + \sin \frac{\theta_k}{2} e^{-i\frac{\phi_k}{2}} q_d = 0, \quad (\text{S36})$$

$$-\sin \frac{\theta_k}{2} e^{i\frac{\phi_k}{2}} p_{-d} + \cos \frac{\theta_k}{2} e^{-i\frac{\phi_k}{2}} q_{-d} = 0. \quad (\text{S37})$$

Now we briefly argue that there always exists θ_k and ϕ_k satisfy equations above. If all p_d, p_{-d}, q_d, q_{-d} are not zero, simply let $\tan\left(\frac{\theta_k}{2}\right) e^{-i\phi_k} = -\frac{p_d}{q_d}$. Then consider the case of zero coefficients. Since $\deg(P) = \deg(Q) = d$, at most two of p_d, p_{-d}, q_d, q_{-d} could be 0. The fact $p_d p_{-d}^* + q_d q_{-d}^* = 0$ implies that one of one of p_d, p_{-d} is 0 if and only if one of q_d, q_{-d} is 0. If $p_d = q_d = 0$ (or $p_{-d} = q_{-d} = 0$), pick θ_k and ϕ_k so that $\tan\left(\frac{\theta_k}{2}\right) e^{i\phi_k} = \frac{q_{-d}}{p_{-d}}$. If $p_d = q_{-d} = 0$ or $(p_{-d} = q_d = 0)$, pick θ_k so that $\sin\left(\frac{\theta_k}{2}\right) = 0$ (or $\cos\left(\frac{\theta_k}{2}\right) = 0$).

Next, for the θ_k that we pick, consider

$$\begin{bmatrix} P & -Q \\ Q^* & P^* \end{bmatrix} W^\dagger(\theta_k, \phi_k) R_Z^\dagger(x) \quad (\text{S38})$$

$$= \begin{bmatrix} e^{i\phi_k/2} \cos \frac{\theta_k}{2} e^{ix/2} P + e^{-i\phi_k/2} \sin \frac{\theta_k}{2} e^{ix/2} Q & e^{i\phi_k/2} \sin \frac{\theta_k}{2} e^{-ix/2} P - e^{-i\phi_k/2} \cos \frac{\theta_k}{2} e^{-ix/2} Q \\ e^{i\phi_k/2} \cos \frac{\theta_k}{2} e^{ix/2} Q^* - e^{-i\phi_k/2} \sin \frac{\theta_k}{2} e^{ix/2} P^* & e^{-i\phi_k/2} \cos \frac{\theta_k}{2} e^{-ix/2} P^* + e^{i\phi_k/2} \sin \frac{\theta_k}{2} e^{-ix/2} Q^* \end{bmatrix} \quad (\text{S39})$$

$$= \begin{bmatrix} \hat{P} & -\hat{Q} \\ \hat{Q}^* & \hat{P}^* \end{bmatrix} \quad (\text{S40})$$

where

$$\hat{P} = e^{i\phi_k/2} \cos \frac{\theta_k}{2} e^{ix/2} P + e^{-i\phi_k/2} \sin \frac{\theta_k}{2} e^{ix/2} Q, \quad (\text{S41})$$

$$\hat{Q} = e^{-i\phi_k/2} \cos \frac{\theta_k}{2} e^{-ix/2} Q - e^{i\phi_k/2} \sin \frac{\theta_k}{2} e^{-ix/2} P. \quad (\text{S42})$$

Since $P, Q \in \mathbb{C}[e^{ix/2}, e^{-ix/2}]$ are Laurent polynomials with degree d , $\hat{P} \in \mathbb{R}[e^{ix/2}, e^{-ix/2}]$ might appear to be a Laurent polynomial with degree $d + 1$. In fact it has degree $\deg(\hat{P}) \leq d - 1$, because the coefficient of $(e^{ix/2})^{d+1}$ term in \hat{P} is $\cos \frac{\theta_k}{2} e^{i\frac{\phi_k}{2}} p_d + \sin \frac{\theta_k}{2} e^{-i\frac{\phi_k}{2}} q_d = 0$ by the selected θ_k and ϕ_k , and the coefficients of $(e^{ix/2})^d$ term is 0 by condition 2. Similarly, \hat{Q} has leading coefficient $-\sin \frac{\theta_k}{2} e^{i\frac{\phi_k}{2}} p_{-d} + \cos \frac{\theta_k}{2} e^{-i\frac{\phi_k}{2}} q_{-d} = 0$ and has degree $\deg(\hat{Q}) \leq d - 1$. Since $d \leq L$, we have $\deg(\hat{P}) = \deg(\hat{Q}) \leq L - 1$, hence condition 1 is satisfied. From the degree parity of P and Q , it is easy to see that \hat{P} and \hat{Q} have degree parity $L - 1 \pmod{2}$,

thus condition 2 is satisfied. Condition 3 follows from unitarity. Thus by the induction hypothesis, Eq. (S40) can be written as a QNN in the form of $U_{\theta, \phi, L-1}^{\text{WZW}}(x)$, and therefore the matrix

$$\begin{bmatrix} P & -Q \\ Q^* & P^* \end{bmatrix} \quad (\text{S43})$$

can be written as a QNN in the form of $U_{\theta, \phi, L}^{\text{WZW}}(x)$. ■

IV. PROOF OF THEOREM 4

Theorem 4 *Let $|\psi(x)\rangle = U_{\theta, \phi, L}^{\text{WZW}}(x)|0\rangle$ and the observable be the Pauli Z operator. For any square-integrable function $f : [-\pi, \pi] \rightarrow [-1, 1]$ and for all $\epsilon > 0$, there exist $L \in \mathbb{N}^+$ and $\theta \in \mathbb{R}^{L+1}, \phi \in \mathbb{R}^{L+1}$ such that*

$$\| \langle \psi(x) | Z | \psi(x) \rangle - f(x) \| \leq \epsilon. \quad (\text{S44})$$

Proof Similar as in the proof of Proposition 2, we use the fact that square-integrable functions f can be approximated by a truncated Fourier series. Then, there exists a $K \in \mathbb{N}^+$ such that

$$\| f_K(x) - f(x) \| \leq \frac{\epsilon}{2}, \quad (\text{S45})$$

where $f_K(x)$ is the K -term truncated Fourier series of $f(x)$. Consider the function $\sqrt{\frac{1+f_K(x)}{2}}$, using the property of square-integrable functions again, there exists an $L \in \mathbb{N}^+$ such that

$$\left\| g_L(x) - \sqrt{\frac{1+f_K(x)}{2}} \right\| \leq \frac{\epsilon}{8}, \quad (\text{S46})$$

where

$$g_L(x) = \sum_{n=-L/2}^{L/2} c_n e^{inx} \quad (\text{S47})$$

is the partial Fourier sum of function $\sqrt{\frac{1+f_K(x)}{2}}$ and $L \pmod{2} = 0$. Next we need to prove

$$\langle 0 | U_{\theta, \phi, L}^{\text{WZW}}(x) | 0 \rangle = g_L(x). \quad (\text{S48})$$

Specifically, $g_L(x)$ can be written as follows

$$g_L(x) = \sum_{n=-L/2}^{L/2} c_n (e^{ix/2})^{2n}. \quad (\text{S49})$$

Obviously, $g_L \in \mathbb{C}[e^{ix/2}, e^{-ix/2}]$ and conditions of Lemma 3 are satisfied, thus Eq. (S48) holds. Further, we have

$$\| \langle \psi(x) | Z | \psi(x) \rangle - f_K(x) \| \leq \frac{\epsilon}{2}. \quad (\text{S50})$$

Finally, combined with inequality (S45), the inequality (S44) holds. ■